ELSEVIER

Marine Geology 244 (2007) 166–183

MARINE GEOLOGY
INTERNATIONAL JOURNAL OF MARINE GEOLOGY, GEOCHEMISTRY AND GEOPHYSICS

www.elsevier.com/locate/margeo

Neogene sedimentary and mass-wasting processes on the continental margin off south-central Chile inferred from dredge samples

Markus Raitzsch *, David Völker [1], Christoph Heubeck

Freie Universität Berlin, Institut für geologische Wissenschaften, Malteserstrasse 74-100, 12249 Berlin, Germany

Received 9 November 2006; received in revised form 11 June 2007; accepted 26 June 2007

Abstract

The active continental margin off south-central Chile (36° to 40°S) is transitional between the tectonically erosive, empty-trench margin north of Juan Fernandez Ridge and the accretionary, trench-filled margin south of the Chile Triple Junction. The small width of the presently active accretionary wedge (maximum width of 25 to 50 km) argues for past phases of tectonic erosion. At present, this sector shows indications of contemporaneous accretion, subduction, and underplating of sediment, as well as readjustment of the slope by various mass-wasting processes.

In this context, this study aims to examine the Neogene sedimentary processes on the continental margin from dredge samples recovered during *R/V SONNE* cruise SO161-5 within this transitional domain using lithology, sandstone petrology, shale mineralogy, and analysis of sedimentary structures. Our results yield that the principal transport of material occurs in high-energy turbidity currents and debris flows via submarine canyons deeply cutting the continental slope, whereas sediment on the shelf is transported by strong coast-parallel bottom currents and trapped by submarine canyons cutting into the shelf. A wide range of mass-wasting processes including slumping, debris flows, evolving to low-density turbidity currents and mud flows, rework the slope sediments. In contrast, thick undisturbed sequences of mostly hemipelagic sediments accumulate in active slope basins, which are largely protected from mass movements.

XRD analyses revealed early diagenetic lithification and overall burial depths of up to ~230 mbsf, suggesting a shallow-subsurface cycle of sedimentation, subsidence, diagenesis, uplift, erosion, and resedimentation. The composition of sandstones is dominated by volcanic rock fragments of Andean provenance. Along-strike modal changes reflect a southward increase in glacially denudation and rainfall, the combination of which caused more intense erosion of volcanic rocks and exposure, weathering and, as a result, increased fluvial transport of metamorphic and plutonic rocks to the sea.

Keywords: south-central Chile; continental slope; submarine sedimentation; mass-wasting; sediment reworking; dredge sample

1. Introduction

The active continental margin off Chile is characterized by the subduction of the Nazca Plate below the South American continental plate (e.g., Dewey and Bird, 1970). Because of its N–S extent and tectonic variability, this margin provides an excellent natural laboratory for the study of the influence of climate, trench fill, age and

* Corresponding author. Present address: MARUM, Universität Bremen, Leobener Strasse, 28359 Bremen, Germany. Tel.: +49 421 218 65663; fax: +49 421 218 65505.
E-mail address: raitzsch@uni-bremen.de (M. Raitzsch).
[1] Present address: Leibniz-Institut für Meereswissenschaften, IFM-GEOMAR, Wischhofstr. 1-3, 24148 Kiel, Germany.

0025-3227/$ - see front matter © 2007 Elsevier B.V. All rights reserved.
doi:10.1016/j.margeo.2007.06.007

thermal state of subducted crust, dip angle of the incoming plate, characteristics of the overriding plate etc. on the development of the forearc.

The cruise of *SONNE* 161-5 studied the 36°–40°S sector (Fig. 1), situated between the tectonically erosive, empty-trench margin (e.g., von Huene and Lallemand, 1990) north of San Fernandez Ridge and the clearly accretionary, trench-filled margin (Bangs and Cande, 1997) south of the Chile Ridge Triple Junction. This sector is intermediate in nature, with latitudinal and probably temporal variations in the volume of subducted, accreted, and underplated sediment (Lohrmann et al., 2006; Ranero et al., 2006; Sick et al., 2006). The small width of the accretionary portion of the continental wedge (25 to 50 km in maximum), identified from seismic profiles, is inconsistent with a continuous history of accretion (Bangs and Cande, 1997). It is therefore reasonable to expect an interaction of frontal accretion, basal accretion, sediment subduction, and readjustment of the slope by various mass-wasting processes in this sector. The factors controlling these variations are described in principle by the critical taper model of Dahlen (1990), but not well known in the special case of south-central Chile.

While there exist numerous geophysical studies on the central Chilean margin (e.g., von Huene et al., 1985; Bangs and Cande, 1997; Díaz-Naveas, 1999; Bohm et al., 2002; Grevemeyer et al., 2003; Ranero et al., 2006; Sick et al., 2006), sedimentary studies are sparse (Thornburg and Kulm, 1987a,b; Scholl et al., 1970; Lamy et al., 1998; Mix et al., 2003; Muñoz et al., 2004). Therefore the fifth leg of the research cruise was carried out with a focus on the characterization of this hybrid convergent margin by geological and geochemical sampling and heat flow measurements.

Our study aims to address the following questions: (1) What is the provenance, age and diagenetic path of shale and sandstones dredged from the continental slope? (2) Which sedimentary processes act or dominate on the continental shelf and slope? (3) Which burial depths of sediments within the accretionary wedge can be reconstructed?

2. Regional setting

The oceanic Nazca Plate is subducting beneath the continental South American plate at an angle of ca. 77°, with a dip angle of approximately 19°, and at an absolute convergence rate of 66 mm/a (e.g., Angermann et al., 1999).

Global seafloor topography (Smith and Sandwell, 1997; Lindquist et al., 2004) and low-resolution, full-coverage bathymetry of the Chilean margin (Zapata, 2001) show a shelf of intermediate width (20–30 km) between 33° and 44°S. Its edge lies at 150 to 250 m below sea level. The continental slope is characterized by small plateaus, lineaments, and escarpments with slopes up to 10° but generally ranging between 2.5° and 4.0° (Zapata, 2001). It shows areas with different slope angles, and can therefore be divided in an upper slope up to 2500 m (2°–3°) and a lower slope between 2500 m and 4600 m (5°–8°) (Vargas, 2005; Vargas et al., 2005). Locally, gently landward-inclined terraces nearly aligned in a N–S direction form potential slope basins.

Ocean Drilling Project Leg 202 (Mix et al., 2003) described sediments from three sheltered slope basins between 36° and 41°S (Sites 1233, 1234, 1235, [Fig. 1]) which were deposited rapidly at average rates of 70–82 cm/ka within the last 260,000 yr. Scholl et al. (1970) calculated a total amount of 105×10^3 km^3 of sediments deposited along the Chilean coast between 36° and 42°S during the entire Cenozoic. Probable cause for such high values is the extremely high terrigeneous sediment supply due to heavy continental rainfall in southern Chile (Lamy et al., 2001). The particular area under discussion between 36° and 40°S forms a transition from moderate (36°S, 90–200 cm rainfall/yr) to humid cold climates (40°S, 450–650 cm rainfall/yr) (Scholl et al., 1970). These conditions provide large quantities of eroded material from the Main and Coastal Cordilleras. Furthermore, several glacial events since 7 Ma, the latest of which is the Llanguihue event 13.9 to 33.5 ka ago (e.g., Mercer, 1976; Rabassa and Clapperton, 1990), contributed to the orogenic denudation and thus to the high availability of continent-derived material.

It is generally assumed that the southern Chilean continental margin was affected by periods of subduction erosion and/or sediment subduction during its long history of convergence for several reasons: (1) The accretionary portion of the wedge has a maximum width of 25 km to 50 km and is therefore comparatively small (Bangs and Cande, 1997). Similarly, the Peruvian accretionary prism also has a width of 20 to 30 km; it is known, that there additional 28 km was consumed by subduction erosion since the Miocene (von Huene and Lallemand, 1990; von Huene et al., 1999). (2) Isotope studies of volcanic arc extrusives indicate a supply of subducted sediments to the arc magma within the last 10 Ma (Sigmarsson et al., 1990; Hickey-Vargas et al., 2002). (3) Long-term sediment mass balances (von Huene and Scholl, 1991) supply evidence that a large volume of trench sediments has been subducted with the downgoing slab. (4) Various geophysical methods indicate the present existence of

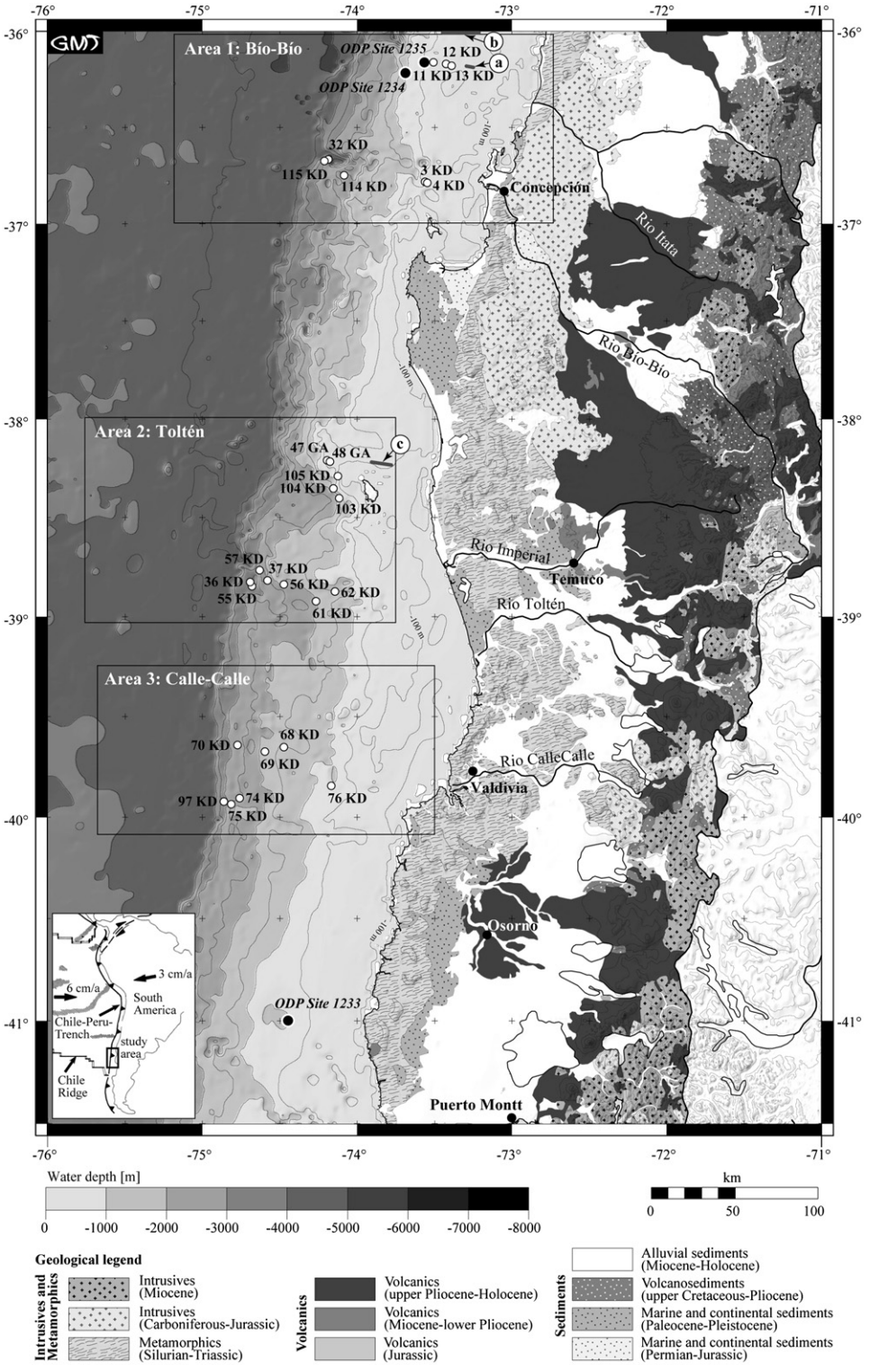

Fig. 1. Bathymetric map off southern central Chile and locations of dredge sampling stations. Investigation subareas of SO161-5 are named after major rivers feeding the prominent submarine canyons. ODP Sites (Leg 202) and PARASOUND profiles from Fig. 9 are indicated as well. Onshore geological units are adopted and simplified from SERNAGEOMIN (2003).

a subduction channel (Ranero et al., 2006; Sick et al., 2006).

The flux of subducted trench sediments is probably related to the opening and closure of this subduction channel. In the area investigated, sediment subduction and accretion seem to act contemporaneously at present.

It has been argued that subduction erosion took place when the trench was not sufficiently filled with sediments to cover the rough relief of the oceanic plate (Bangs and Cande, 1997). This general idea seems to be true at present for the general distinction between northern Chile (erosive) and southern Chile (partly accretive). Therefore, in the area investigated, the change between accretionary and tectonically erosive phases of subduction was probably controlled mainly by changes in the sediment supply to the trench.

There are several indications for recent vertical uplift of the marine and coastal forearc in places: (1) Heat flow values are extremely low and make a steady-state unlikely (Ferguson et al., 1993; Hyndman et al., 1993; Wiedicke-Hombach and Shipboard Scientific Party, 2002; Grevemeyer et al., 2003). (2) The interpretations of reflection seismic data of Bangs and Cande (1997) and Díaz-Naveas (1999) show that the south-central Chilean accretionary wedge grew rapidly vertically within the last 1 to 2 Ma, possibly as a result of sediment underplating beneath the prism, amplified by very high sedimentation rates on the continental slope. (3) Lohrmann et al. (2006) argue that a portion of the strong surface uplift of 0.8–5.5 mm/yr in the Arauco Peninsula area, documented by paleoshorelines, is explicable by tectonic underplating. (4) Melnick and Echtler (2006) claim a ~1.5 km rise of the shelf during the middle Pliocene due to a forearc basin inversion associated with changes in the mechanical properties of the margin wedge as a response to rapid increase of glacial age sediment supply to the trench.

Six major (and some minor) submarine canyon systems transect shelf and continental slope in the study area where they cut up to 1000 m into the middle slope (Fig. 1). From south to north, these are the Bueno, Calle-Calle, Toltén, Imperial, and Bío-Bío canyons. The path of the Bío-Bío canyon is controlled by the Bío-Bío fault zone, one of the three main fault systems. The canyon is in an active erosion phase, which produces the migration of the canyon head towards the continent, now located at a depth of 15–20 m and a distance of 300 m from the shoreline (Pineda, 1999). This has a significant effect on the sedimentation–erosion equilibrium of Escuadrón beach since the Bío-Bío river will discharge directly to the canyon, and the sedimentary contribution to the beach will decrease (Pineda and Fanucci, 1994; Pineda, 1999). Further north, three unnamed canyons and the large San Antonio canyon off Valparaiso possibly form additional major sedimentary pathways to the trench (Thornburg et al., 1990; Laursen and Normark, 2002). The mean spacing between canyons along the coast is 70–100 km. The larger canyons commence on the shelf and feed directly off large river mouths (Zapata, 2001).

At the downslope exits of most of the larger canyons, submarine fan systems exist (Thornburg et al., 1990). These submarine fans exhibit a constructive (possibly Pleistocene) and a destructive (possibly present) phase (Thornburg et al., 1990; Völker et al., 2006).

The trench in the area under discussion has only a weak morphological expression, owing to the copious sedimentary infill. Instead, a flat, broad plain, some 25–100 km across, is observed (Fig. 1). The trench plain is gently inclined to the north whereby its average depth increases from 4500 m at 42°S to 5400 m at 36°S (Smith and Sandwell, 1997; Lindquist et al., 2004). In seismic sections across the trench, the sediment fill is visible as a seaward-thinning, wedge-shaped deposit, formed by subhorizontal strata that onlap the sedimentary cover of the Nazca Plate (von Huene et al., 1997; Laursen and Normark, 2002; Rauch, 2005). This sedimentary sequence is approximately 2–2.5 km thick and predominantly composed of turbidites (Bangs and Cande, 1997; Laursen and Normark, 2002; Mix et al., 2003).

The most prominent feature within the morphologically flat area of the trench sediment is formed by a S–N-trending channel, the Chile Trench Axial Channel (Thornburg and Kulm, 1987a; Laursen and Normark, 2002; Völker et al., 2006). The channel cuts into the sedimentary fill of the trench plain and shows the same northward inclination. Submarine fan distributary channels emanate in the trench axial channel (Thornburg and Kulm, 1987a; Völker et al., 2006).

A detailed study of petrofacies and provenance from modern south-central Chilean trench sediments distinguished three main petrofacies (Thornburg and Kulm, 1987b): (1) *Basic magmatic arc petrofacies* from the Main Cordillera, incl. olivine, pyroxene, plagioclase, and volcanic rock fragments with a Pliocene to Quaternary of basaltic and andesitic magmatic arc provenance. (2) *Acidic magmatic arc petrofacies*, incl. quartz, K-feldspar, hornblende, biotite, and opaque minerals (magnetite), representing a mixture of pre-Pliocene volcanic and plutonic provenance. (3) *Metamorphic complex petrofacies*, incl. chlorite, mica, green hornblende, epidote, actinolite, apatite, K-feldspar, quartz, and metamorphic rock fragments. Corresponding Paleozoic source rocks are located in the Coastal Cordillera and mainly form part of a Late Paleozoic accretionary complex.

The area under discussion shows a high seismicity, documented by megathrust-earthquakes like the Valdivia earthquake of 1960, with a magnitude of 9.5 the largest one ever recorded (Plafker, 1972). It seems plausible that such hazards trigger mass-wasting processes on the slope and thus influence the morphology of the continental slope.

3. Materials and methods

A total of 89 rock samples of a variety of lithologies of sedimentary origin were recovered with a chain-bag dredge from 27 stations (Fig. 1 and Table 1) on the continental slope and on the outer shelf. They were investigated for macroscopic sedimentary structures, sandstone petrographic composition, and bulk composition by X-ray diffraction analysis. During the cruise, the PARASOUND multibeam swath echosounder was operated continuously, and provided additional information on the sedimentary environment. Biostratigraphic ages of some samples could be determined with nannofossil analyses (Wiedicke-Hombach and Shipboard Scientific Party, 2002) using the stratigraphies of Young (1998) for the Neogene, of Hine and Weaver (1998) for the Quaternary, of Perch-Nielsen (1985) for the entire Cenozoic, and of Barron (1985) for the Miocene to Holocene (Table 1).

The sampling strategy was aimed to obtain samples from the entire width of the continental margin including outer shelf, submarine slope, and floor and walls of submarine canyons. Due to the nature of the dredging process, by which the weighted chain sack is hauled across the sea bottom, a sample of the outcropping lithologies is obtained, preselected for lithologic hardness, submarine outcrop ruggedness, and orientation of the dredge haul with respect to structural trend. It has to be considered that the exact location of samples with respect to their original depositional environment is somewhat reduced by tectonic and sedimentary reworking processes.

3.1. Sandstone petrography

Eleven thin sections from eight well-lithified medium-grained sandstones (sampling locations: 11 KD, 36 KD, 37 KD, 55 KD, 56 KD, 57 KD, 75 KD, 97 KD) were examined for their petrographic composition and subsequently interpreted for provenance analysis. For each thin section, 400 to 500 framework grains were point-counted following Gazzi and Dickinson (Gazzi, 1966; Ingersoll et al., 1984; Dickinson, 1985). Accordingly, grains were classified as monocrystalline (Qm) and polycrystalline quartz (Qp), chert (Qch), plagioclase (P), K-feldspar (F), volcanic rock fragments (Lv), sedimentary rock fragments (Ls), metamorphic rock fragments (Lm), mica, and “others”.

3.2. Bulk and clay mineralogy

Ten samples of mostly silty character from five sampling sites (sampling locations: 37 KD, 55 KD, 56 KD, 61 KD, 62 KD) were prepared for X-ray analysis, principally following the method of Kisch (1991). Bulk mineralogy was analyzed by scanning the powdered whole rock material from 3° to 70° 2θ (2ϑ). The clay-sized fraction (<2 μm) was separated by the Atterberg method, and prepared in smear slides with a layer density of 2 mg/cm^2, in accordance with recommendations of Arkaí (1991), Eberl et al. (1987), and Lezzerini et al. (1995).

After a scan on the air-dry state from 3° to 40° 2θ, preparations were treated with ethylene glycol and X-rayed from 3° to 20° 2θ in order to detect expandable layers in mixed-layer clay minerals. All measurements were performed on a Philips PW 1710 (CoKα radiation, I=30 mA, U=40 kV, software PC-APD). Measured FWHM (Full Width at Half Maximum) values were calibrated with standardized CIS values from Warr and Rice (1994). The diffractograms were smoothed, corrected, and analyzed by the MacDiff 4.2.5 software (Petschick, unpubl.). The clay mineral composition was determined by using a semi-quantitative method revised by Braukmann (1984). Accordingly, the peak areas of main basal reflections were weighted in the glycolated state using smectite (17 Å), illite (10 Å), and kaolinite/chlorite (7 Å).

4. Results

4.1. Sedimentology

Neither metamorphic nor igneous rocks of continental basement nor oceanic crust-affinity was obtained during the sampling program, although we intentionally dredged from walls of up to 1 km deeply incised submarine canyons with lack of a recent sedimentary cover. None of the samples could be dated older than early Miocene. The oldest samples were mainly found on the upper slope and the outer shelf (Table 1). All recovered samples are exclusively of sedimentary origin, dominantly clastic, and commonly with characteristic sedimentary structures indicative of a variety of sediment transport and depositional processes. Most samples from the upper slope (to 2500 m water depth) and from the shelf are bioturbated to a variable degree. Bioturbation

Table 1
Summary of sampling stations with short description of recovered rock types, lithologies, and nannofossil ages

Sample	Longitude (S)	Latitude (W)	Water depth (m)	Target	Rock types/Lithology (age from nannoplankton analysis)
Area Bío-Bío					
3 KD	36°46.34′–36°46.69′	73°33.55′–73°33.08′	974–600	Bío-Bío canyon	Hardgrounds of laminated mudstones, occasionally interbedded with distal turbidites (*Neogene*)
4 KD	36°46.54′–36°46.59′	73°32.10′–73°32.96′	695–510	Bío-Bío canyon	Similar to 3 KD
11 KD	36°09.09′–36°09.37′	73°30.49′–73°30.10′	184–163	Shelf	(1) Medium- to coarse-grained Ta litharenites with claystone clasts (2) Fine- to medium-grained Tb/c litharenites with planar or ripple-drift cross lamination
12 KD	36°09.63′–36°09.72′	73°25.66′–73°25.33′	126–123	Shelf	Grey mudstones interbedded with fine- to medium-grained Tb/c sandstones, planar lamination, dewatering structures (*Neogene with reworked Paleogene*)
13 KD	36°10.17′–36°10.60′	73°23.48′–73°22.99′	120–117	Shelf	(1) Bioturbated siltstones (2) Tuff horizons with lapillis and bentonite layers
32 KD	36°39.26′–36°39.64′	74°11.05′–74°10.56′	3595–3165	Bío-Bío canyon	Fine- to medium-grained turbiditic litharenites with claystone clasts
114 KD	36°44.70′–36°43.93′	74°04.70′–74°04.85′	2881–2563	Bío-Bío canyon	(1) Well-sorted, fine-grained Tb/c/d sandstones, occasionally with ripple-drift cross lamination, load balls and flame structures (2) Sandstone–mudstone couplets (3) Massive mudstones interbedded with sandy horizons (*lower Quaternary*) (4) Fine-grained sandstones with horizontal stratification (Fig. 4c)
115 KD	36°39.80′–36°40.05′	74°12.58′–74°12.14′	3596–3246	Bío-Bío canyon	(1) Fine- to medium-grained Ta sandstones with clay-rich matrix (greywacke) (2) Sand-bearing turbiditic siltstones interbedded with fine-grained sandstones (*Neogene*) (3) Fractured grey mudstones
Area Toltén					
36 KD	38°49.48′–N/A	74°40.50′–N/A	3723–3340	Toltén canyon	(1) Turbiditic litharenites with ball-and-pillow structures, convolute bedding, flame structures (2) Polymict clay-clast conglomerates (3) Mudstones (*Neogene*)
37 KD	38°47.76′–38°48.19′	74°34.49′–74°34.24′	2343–2061	Toltén canyon	Massive, poorly sorted, and quartz-veined Ta litharenite
47 GA	38°11.52′	74°11.60′	208	Shelf	Well-lithified, silty limestones with ash particles and shell fragments
48 GA	38°11.88′	74°10.45′	224	Shelf	Similar to 47 GA (*Pleistocene*)
55 KD	38°48.23′–38°48.85′	74°41.27′–74°41.57′	4054–3603	Toltén canyon	(1) Fine- to coarse-grained litharenites (*late Pliocene to Pleistocene*) (2) Bioturbated pellet-rich siltstones (*middle Miocene to late Pliocene*) (3) Clay-rich fine-grained sandstones
56 KD	38°48.98′–38°48.74′	74°28.21′–74°28.59′	1729–1420	Upper slope	(1) Massive mudstones from mud turbidites and mud flows (*Pleistocene*) (2) Clay-rich siltstones with ripples and convolute bedding (*middle Pliocene to Holocene*) (3) Medium- to coarse-grained Ta and Tc turbidites (Fig. 4b) (4) Fine- to medium-grained turbiditic sandstones
57 KD	38°44.69′–38°44.04′	74°37.59′–74°36.80′	3314–2625	Lower slope	(1) Graded, fine-grained turbiditic sandstones (2) Sandy mudstones and clayey siltstones
61 KD	38°53.99′–38°53.65′	74°15.82′–74°15.90′	1946–1601	Toltén canyon	(1) Clay-clast conglomerates grading into coarse-grained sandstones (2) Bioturbated clay-rich siltstones (*middle Pliocene to Holocene*) (3) Laminated turbiditic siltstones with convolute bedding (*Pleistocene to Holocene*) (4) Clayey fine-grained sandstones with flame structures
62 KD	38°51.44′–38°51.07′	74°08.31′–74°08.54′	1153–829	Upper slope (anabranch of Toltén canyon)	(1) Clay-rich siltstones (*early Quaternary*) (2) Fine- to medium-grained turbidites with ripple-drift cross lamination and flame structures (Fig. 3b) (3) Fine-grained Tc/d turbidites with convolute bedding
103 KD	38°23.02′–38°22.54′	74°06.90′–74°06.52′	519–180	Upper slope to shelf	Bioturbated clay- and sand-bearing siltstones (*Miocene*)
104 KD	38°20.01′–38°19.99′	74°09.15′–74°09.01′	580–390	Upper slope	(1) Massive claystones with laminated cross-bedded Tb/c sandstone lenses (*Pliocene to Pleistocene*)

(continued on next page)

Table 1 (*continued*)

Sample	Longitude (S)	Latitude (W)	Water depth (m)	Target	Rock types/Lithology (age from nannoplankton analysis)
					(2) Polymict, matrix- to grain-supported conglomerates (3) Well-rounded, pebble- and cobble-sized clasts of andesitic/tholeiitic origin
Area Toltén					
105 KD	38°16.30′–38°16.42′	74°07.40′–74°06.96′	164–105	Shelf	(1) Bioturbated hardgrounds of grey laminated mudstones interbedded with fine- to medium-grained turbidites (*early Miocene*) (2) Well-rounded gravels, derived from continental metagranitoids, quartz-rich intrusives, and tholeiitic basalts (Fig. 2) (3) Mud-rich limestones with volcanic ash particles and shell fragments (similar to 47 GA and 48 GA) (4) Fine-grained tempestites
Area Calle-Calle					
68 KD	39°37.59′	74°28.19′	1917	Calle-Calle canyon	(1) Clay-rich debrites interbedded with fine-grained sandstone lenses (*Pleistocene*) (2) Massive siltstones to very fine-grained sandstones (*lower Quaternary*)
69 KD	39°38.97′	74°35.56′	2350	Calle-Calle canyon	(1) Bioturbated, pellet-bearing siltstones (*middle Pliocene to Holocene*) (2) Mudstones interbedded with fine-grained sandstones and convolute bedding (3) Bioturbated, very fine-grained sandstones
70 KD	39°37.01′	74°46.10′	2998	Calle-Calle canyon	(1) Clay-rich siltstones, rich in foraminifera (*lower to upper Pliocene*) (2) Graded silt/sandstones with flame structures (*upper Pliocene to Pleistocene*) (3) Clayey to silty debrites interbedded with Tc turbidites, ball-and-pillow structures (*lower Pliocene to Pleistocene*)
74 KD	39°52.79′	74°45.26′	2700	Lower slope	(1) Massive, clay-rich and mica-bearing mudstones (middle Pliocene to Pleistocene) (2) Clay-rich siltstones with fine-grained sandstone wisps
75 KD	39°54.51′–39°55.02′	74°48.58′–74°48.66′	3334–2895	Bueno canyon	(1) Middle- to coarse-grained Ta litharenites (2) Fine-grained, clay-rich litharenites with dish-and-pillar structures (from liquefied flows?) (3) Plastic, cohesive, clayey silts
76 KD	39°49.10′–39°49.11′	74°09.91′–74°10.07′	1000–900	Calle-Calle canyon	(1) Siltstones to fine-grained Tc/d sandstones with ripple-drift cross bedding and slump folds (Fig. 4a) (*middle Pliocene to Pleistocene*) (2) Polymict conglomerates with fluvially derived clasts
97 KD	39°53.80′–39°54.07′	74°51.40′–74°51.22′	3800–3551	Bueno canyon	Fine- to medium-grained Ta litharenites with clay-rich matrix (greywacke)

is apparent from the occurrence of trace fossils (e.g., burrows) and destruction of primary sedimentary fabric which did partly result in complete homogenization of fine-grained sedimentary rocks in samples obtained from shallow water depths. The dredge samples recovered in each area studied comprise different rock types and lithologies as follows (see also Table 1):

4.1.1. Bío-Bío area

The samples from the *outer shelf* consist of medium- to coarse-grained Ta or fine to medium Tb/c litharenites (Bouma division), occasionally with claystone clasts and planar or ripple-drift cross lamination (11 KD). In addition, bioturbated mudstones (13 KD) were dredged, in some cases interbedded with fine- to medium-grained Tb/c sandstones and with planar lamination and dewatering structures (12 KD). Furthermore, we found tuff horizons containing moderately rounded lapillis and bentonite layers (13 KD).

Many samples from the Bío-Bío *canyon* represent laminated or massive mudstones (115 KD) which might be interbedded with fine-grained distal turbidites (3 KD, 4 KD, 114 KD [Fig. 4c], 115 KD). Recovered turbiditic sequences consist of fine- to medium-grained Ta litharenites (115 KD), in one case with claystone clasts at the base (32 KD), and fine-grained Tb/c/d sandstones with horizontal stratification or ripple-drift cross lamination, load balls and flame structures (114 KD).

4.1.2. Toltén area

The *outer shelf* samples comprise bioturbated and well-lithified mud-rich limestones with volcanic ash particles and shell fragments (47 GA, 48 GA, 105 KD), and hardgrounds of grey laminated mudstones interbedded with fine- to medium-grained turbidites (105 KD) which are similar to those recovered in the Bío-Bío area. Additionally, loose well-rounded gravels derived from continental metagranitoids, quartz-rich intrusives, and

tholeiitic basalts (105 KD, Fig. 2), fine-grained tempestites (105 KD), and semi-consolidated cohesive silty clays or clayey silts were dredged.

On the *upper slope*, massive clay-rich or sand-bearing mudstones (56 KD, 62 KD, 103 KD) were retrieved, in some cases with ripples and convolute bedding (56 KD) or lenses of laminated cross-bedded Tb/c sandstones (104 KD). Also, a variety of turbiditic sequences was obtained ranging from medium- to coarse-grained Ta and Tc turbidites (56 KD, Fig. 4b) to fine- to medium-grained Tc/d sandstones (56 KD) with ripple-drift cross lamination and flame structures (62 KD, Fig. 3b), or with convolute bedding (62 KD). Furthermore, matrix- to grain-supported polymict conglomerates as well as loose well-rounded, pebble- and cobble-sized clasts of andesitic/tholeiitic origin (104 KD) were dredged.

The samples from the *lower slope* (57 KD) consist of graded fine-grained turbiditic sandstones, sandy mudstones, and clayey siltstones.

In the Toltén *canyon* turbidite sequences ranging from massive, poorly sorted, and quartz-veined Ta litharenites (37 KD, 55 KD) through Tc litharenites with ball-and-pillow structures, convolute bedding, and flame structures (36 KD, 61 KD) to laminated Td siltstones with convolute bedding (55 KD, 61 KD) were recovered. Also, clay-clast conglomerates (36 KD, 61 KD) and bioturbated mudstones (36 KD, 55 KD, 61 KD) were sampled.

4.1.3. Calle-Calle area

The samples from the *lower slope* (74 KD) comprise massive, clay-rich and mica-bearing mudstones and clay-rich siltstones containing fine-grained sandstone lenses (Fig. 3a).

The samples from the Bueno and Calle-Calle *canyons* reveal a variety of mass flow deposits like clayey to silty debrites interbedded with fine-grained Tc sandstones (68 KD, 69 KD, 70 KD), fine- to medium-grained Ta litharenites (75 KD, 97 KD), fine-grained Tc/d sandstones or siltstones with flame structures, ripple-drift cross bedding and slump folds (69 KD, 70 KD, 76 KD [Fig. 4a]), and fine-grained, clay-rich litharenites with dish-and-pillar structures, possibly deposited from liquefied flows (75 KD). Also, numerous samples consist of clay-rich siltstones, occasionally rich in pellets or foraminifera (69 KD, 70 KD), as well as plastic and cohesive clayey silts (75 KD). Furthermore, polymict conglomerates with fluvially derived clasts were among dredge samples (76 KD).

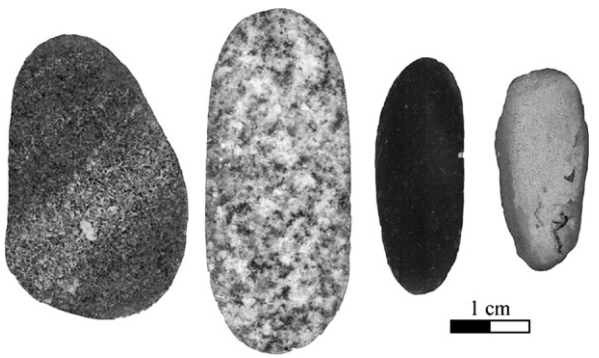

Fig. 2. Some sawed and polished, well-rounded gravels from 105 KD showing a variety of different source rocks. From left to right: chloritized metagranitoid, quartz-rich intrusive, tholeiitic basalt, ash-bearing siltstone.

4.1.4. Early lithification and deformation

Most samples from all studied areas are deformed to various degrees and in different styles. Deformation in unconsolidated sediments is represented by slump folds (Fig. 4a) and water-escape structures (convolute bedding, flame-, ball-and-pillow-, and dish-and-pillar structures). Increased lithification is indicated by a deformation pattern where the sediment is partly folded, but also disrupted by faults which in turn are filled by sediment (Fig. 4b). Progressive lithification is visible by brittle fractures (e.g., joints, fault surfaces with offsets, Fig. 4c) and calcite veining. Several of the recovered samples were lithified and deformed in a brittle manner shortly after deposition. Early brittle response is indicated by brittle faults offsetting lamination by mm or at most few cm. These microfaults end abruptly at horizontal stratigraphic contacts (Fig. 3a, detail I) and indicate that lithification was an early and surficial process that occurred penecontemporaneously with sedimentation.

4.1.5. Reworking

Many sediment samples, both from the submarine canyons and the slope, may have undergone more than one episode of transport and sedimentation, exhibiting evidence of erosion, transport, and resedimentation in mass flows. In these cases, mass flow deposits contain lithological and textural relicts of the incorporated lithofacies (Fig. 3a, detail III). At the contact of different lithofacies, load and dewatering structures are apparent (Fig. 3b, detail II). Furthermore, many dredge samples also appear to be eroded from previously consolidated rocks which can be seen in weathering rinds (partly with slickensides).

4.2. Sandstone petrography

In medium-grained sandstones, volcanic rock fragments are the most abundant particles and contribute to

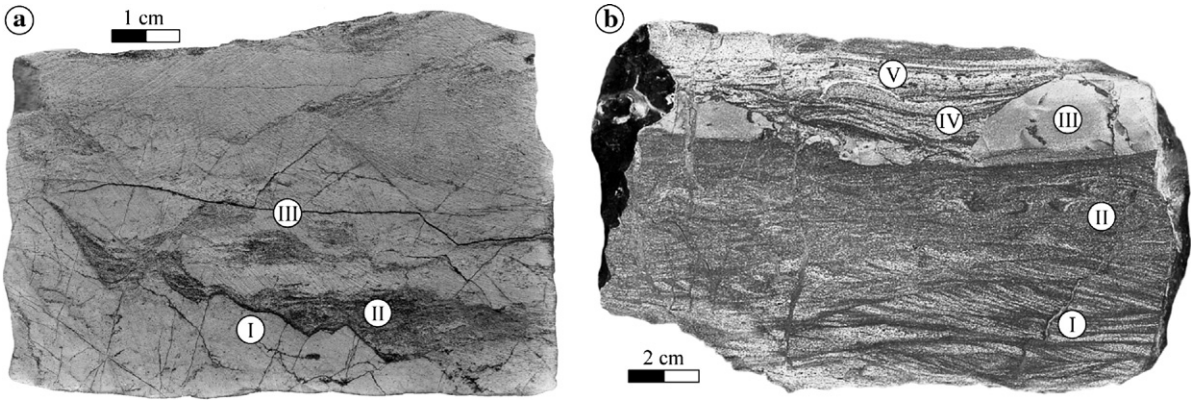

Fig. 3. Two examples for erosive and reworking mass flow deposits. a) 74 KD: a mud flow deposit with brittle fractures (I), maybe due to early diagenetic lithification, followed by a laminated distal turbidite (II). A subsequent mass flow eroded parts of the turbiditic sequence, thus with sandy wisps remaining as relicts in the overlying mud flow (III). b) 62 KD: at the base turbiditic Bouma-Tc sequence with ripple-drift-cross lamination (I), and followed by flame structures (II). This sequence is bounded by an erosional contact, subsequent Ta clasts (III) and planar laminated Tb sands (IV), and an oriented shell (V).

1/4 to 1/2 of the point-counted framework grains (mean 39%) (Fig. 5). They consist mostly of unoriented plagioclase crystals floating in a finely crystallized matrix of plagioclase and pyroxene. These andesitic basalts are typical of the modern volcanic arc rocks in the Chilean Andes (e.g., Deruelle, 1982). Other volcanic rock fragments consist of glassy (sub-) volcanics, seen as opaque grains under crossed nicols. The proportion of volcanic rock fragments distinctly decreases southward from 52% in the Bío-Bío area to less than 25% in the Calle-Calle region.

Plagioclase is the second-most dominant mineral group (approximately 20%). Its proportion shows a southward increase from less than 18% in the northernmost area to more than 26% in the south. Proportions of K-feldspar and monocrystalline quartz do not change appreciably with latitude, and contribute approximately 6% and 8% of the grains, respectively, comparable with chert fragments at ~6% similar. In comparison to monocrystalline quartz and chert fragments, polycrystalline quartz is with 4% less abundant, but its proportion grows southward from 1% in the Bío-Bío area to about 6% in the Calle-Calle area.

Metamorphic rock fragments include mica schists and altered granitoids, altered tholeiitic basalts, and altered volcaniclastics. Their proportions increase southward from approximately 2% in the Bío-Bío area to more than 10% in the Calle-Calle area.

Sedimentary rock fragments include silty clays and clayey silts, which may represent reworked slope and shelf sediments. They contribute approximately 3% of the total content in general, with a maximum of 5% in

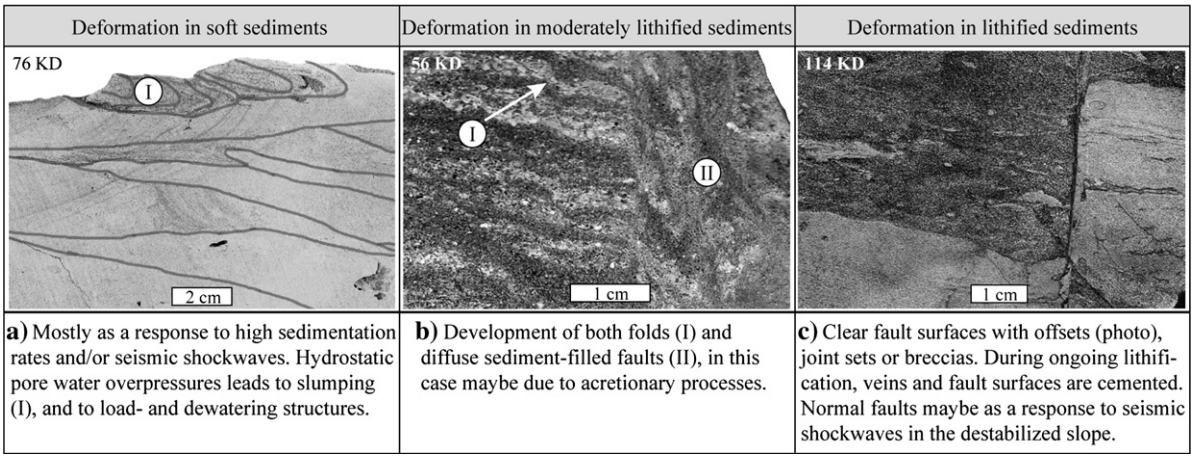

Fig. 4. Different deformation styles due to different degrees of lithification. The spectrum ranges from softsedimentary to brittle deformation.

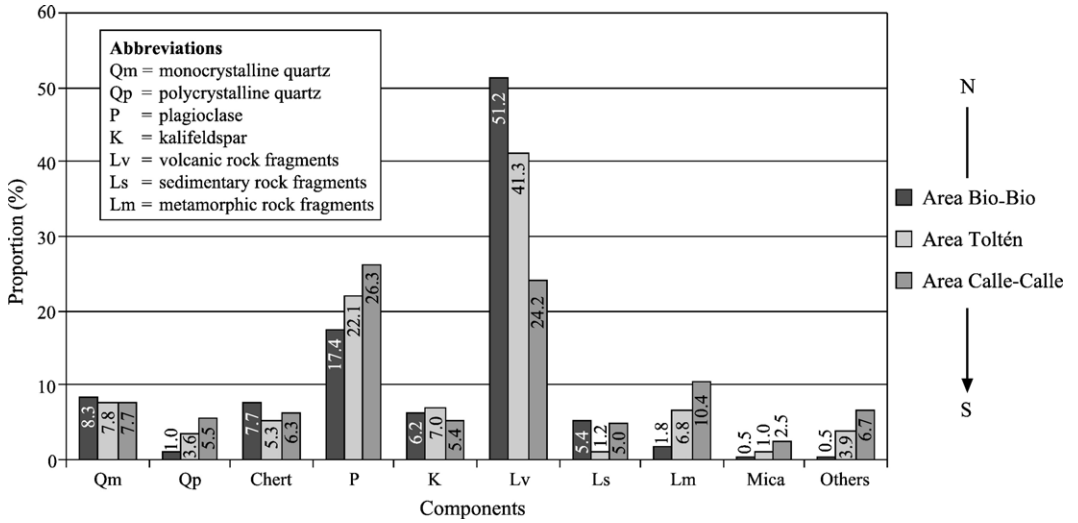

Fig. 5. Bar graph of sandstone compositions, averaged for each segment investigated. Volcanic rock fragments are the most abundant components, showing a proportion decreasing southward. In contrast, the proportions of polycrystalline quartz, plagioclase, and metamorphic rock fragments increase southward, reflecting the southward increase of precipitation and thus of Andean denudation.

the southern and northern areas. In the Toltén transect, sedimentary rock fragments do not contribute to the sandstone composition significantly.

Remaining framework grain components are composed of micas and "others". The latter include heavy minerals such as epidote, zircon, hornblende, pyroxene, apatite, opaque minerals like magnetite, and occasionally hematite. Chlorite, green hornblende, epidote, actinolithe, apatite, and zircon indicate an origin from greenschist-facies rocks. The contribution of "others" does not exceed ~7% which is reached in the Calle-Calle area. The amount of mica is generally low and reaches its maximum of about 3% in the southernmost region (Fig. 5).

All sandstones from the lower slope are characterized by similar QFL-ratios and are classified after Homrighausen (1979) as greywackes (Fig. 6a). The QFL and QmFLt ratios (Fig. 7) are very similar and indicate an undissected to transitional magmatic arc provenance.

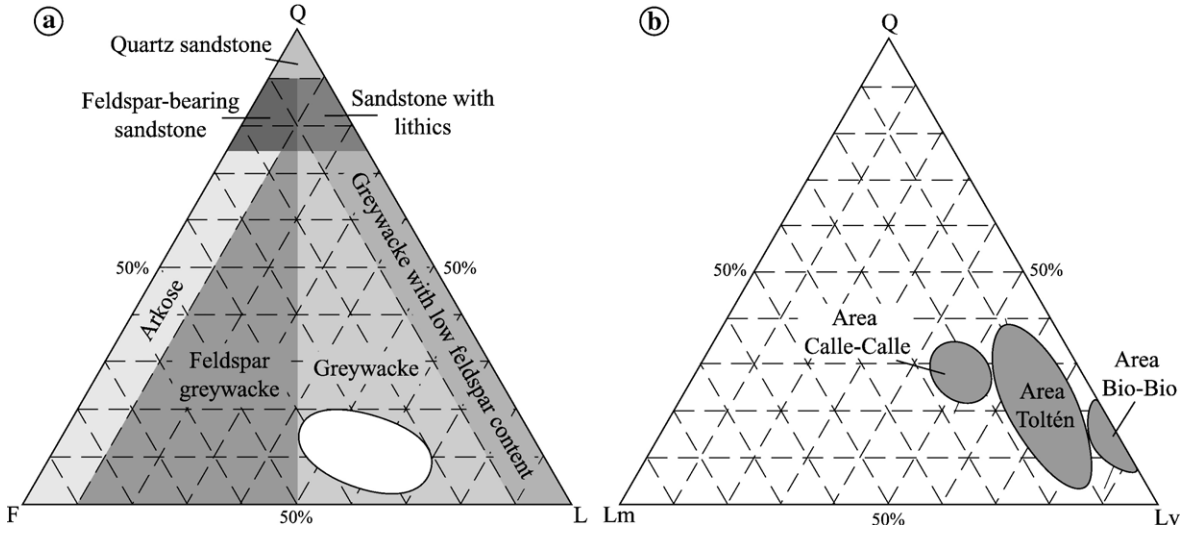

Fig. 6. a) QFL diagram after Homrighausen (1979). All recovered sandstones from the lower slope are classified as greywackes. (Q=Qm+Qp; F=P+K; L=Lv+Lm+Ls). b) QLmLv diagram shows a southward decrease of volcanic rock fragments, and a southward increase of metamorphic rock fragments, due to the southward increase of denudation of the hinterland.

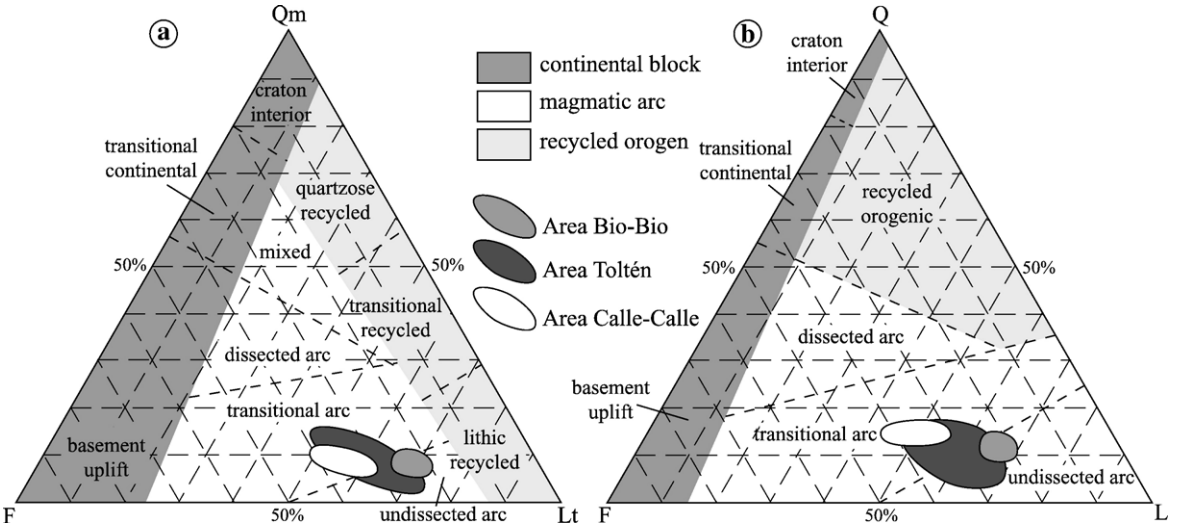

Fig. 7. a) QmFLt (Lt=Qp+Chert+L) and b) and QFL diagrams indicate an undissected to transitional arc provenance (after Dickinson, 1985), reflecting a high input from the Andean magmatic arc. Quartz contents are generally low (<15%), the proportion of lithics (L) is approximately 60%, and that of feldspar (F) ca. 30%.

The QLmLv data (Fig. 6b) show that the proportion of metamorphic rock fragments increases southward from less than 10% to up to 25%. Even the amount of metamorphic heavy minerals like epidote, zircon, hornblende, pyroxene, and apatite increases southward. Correspondingly, the ratios of volcanic rock fragments decrease southward from 80% to 50%. The proportion of quartz shows an increase from 15% in the north to 30% in the south.

4.3. X-ray diffractometry

Dredge sites of samples selected for XRD analysis lie in the Toltén area along an E–W trending transect across the continental slope (Fig. 8). The samples of mostly silty character are from the submarine canyon (37 KD, 55 KD, 61 KD) and from the slope (56 KD, 62 KD).

The bulk mineralogy, determined by XRD measurements, includes albite, anorthite, orthoclase, quartz, chlorite, muscovite, biotite, hornblende, pyroxene, and calcite. In one sample (62 KD, Fig. 3b), calcite was completely replaced by dolomite, and some diffractograms show subtle peaks at 1.63 Å, 2.71 Å, and 2.43 Å, suggesting low pyrite contents.

Smectite, chlorite, and illite are the principal clay minerals in all samples. Kaolinite and mixed-layer clays do not contribute significantly. The amount of expandable smectite layers in illite does not exceed 15%. Illite is well-crystallized (FWHM 0.25° 2θ to 0.42° 2θ) and predominantly characterized by a muscovitic chemistry and by K as dominant inter-layer cation.

Clay mineral composition shows a well-defined zonation with sample longitude (Fig. 8). The chlorite proportion increases from 22% on the lower slope to 51% on the upper slope, whereas the proportion of smectite correspondingly decreases from 74% to 38%. The illite proportion is generally low and reaches its maximum of 22% on the middle slope.

5. Discussion

5.1. Provenance, sedimentation, and sediment reworking

5.1.1. Lm–Lv ratio

Our study on samples of Neogene age reveal latitudinal changes in the sandstone composition, and

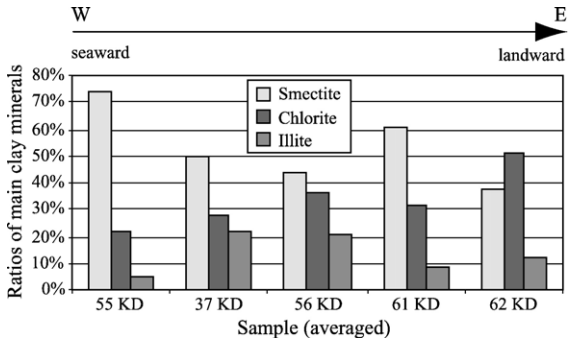

Fig. 8. Bar graph showing proportions of smectite, chlorite, and illite, which are forming the main clay mineral composition. With increasing distance from the coast, the proportion of smectite increases, and that of chlorite decreases. Both may be related to different flocculation efforts and thus to different settling times.

temporal changes with respect to modern sediments studied by Thornburg and Kulm (1987b). QFL and QLmLv diagrams of samples from the lower slope (Fig. 6) show latitudinal changes in terms of a southward increase of metamorphic rock fragments and a corresponding relative decrease of volcanic rock fragments. We attribute these latitudinal trends to the southward increasing orogenic denudation related to the southward increase of Pleistocene glaciation and of Holocene precipitation rates. Both have caused erosion of surface volcanic rocks exposing metamorphic and plutonic rocks, material of which is transported to the sea. These results are consistent with the provenance study of Thornburg and Kulm (1987b) from modern trench sands except that in this study we found slightly lower feldspar and quartz contents. These differences can be attributed to the age distribution of our samples (which include material late Tertiary in age) and their samples, confined to modern sediment. Our database therefore probably reflects a reduced, in part pre-Pleistocene level of Andean downcutting and erosion, and a resulting higher proportion of volcanic rock fragments.

5.1.2. Thin sedimentary cover on the shelf

PARASOUND records (Fig. 9) indicate that the shelf in the study area is characterized by an extremely thin cover or even an absence of unconsolidated sediments. Outer shelf sediments only reach 5 to 10 m thickness (Wiedicke-Hombach and Shipboard Scientific Party, 2002). The bathymetric data of Zapata (2001) show that the Bío-Bío, Toltén and Calle-Calle canyons cut into the shelf which serve as potential sediment traps. Due to an active erosion phase, the head of the Bío-Bío canyon was migrating towards the continent up to its present position, 300 m from the coast (Pineda, 1999). The strong poleward Gunther Undercurrent (or Poleward Undercurrent, PUC; (e.g., Strub et al., 1998; Zapata, 2001) at 0.2–0.5 km water depth flows close enough to the edge of the shelf to induce coast-parallel southward sediment transport. Current velocities ranging from 0.1 to 0.5 m/s at depths of 100–300 m were measured with a variety of methods (Huyer et al., 1991; Pizarro et al., 2002). Shaffer et al. (1999), Shaffer et al. (1997), and Shaffer et al. (1995) reported a mean value of 0.128 m/s and a maximum value of 0.689 m/s over a period of 6 yr. Consequently, neither fluvially-delivered nor longshore-delivered sediment are distributed on the shelf.

5.1.3. Sedimentation pattern on the outer shelf

The oldest sediments (Miocene, in one case with reworked Paleogene) were found on the outer shelf and the uppermost slope (Table 1). Hence, we interpret the outer shelf samples as residual sediments of Tertiary age which underlie the thin unconsolidated sedimentary cover. They support our assumption that material with a grain size smaller than gravel transported along the shelf is mostly funneled by the submarine canyons. Only winnowed gravel lags remain as principal relicts. Lamy et al. (1998), studying modern shelf and slope sediments at the 36°S transect, found that outer shelf and the uppermost-slope sediments were coarser grained than those from the lower slope and in the very nearshore areas. They attributed this result to winnowing by bottom currents and/or resedimentation processes.

Distinctive black volcanic sands form an alluvial fan of approx. 50×60 km^2 size in the central valley of Chile (*arenas negras de Trupán-Laja*; Thiele et al., 1998). These deposits were interpreted as the product of a catastrophic flooding event caused by the collapse of a natural dam of the Lago de Laja at 9700 ± 600 ybp (Thiele et al., 1998). A speculative correlation of these deposits with the black sand in several shelf samples needs to be confirmed by a future comparative petrographic study.

5.1.4. Sedimentation on the slope

The slope sediments are of Pliocene to Pleistocene age (Table 1) and thus younger than the Miocene lithologies outcropping at the shelf and the uppermost slope. Even the samples dredged from walls of the deeply incised canyons (up to 1000 m below the general slope surface) are mostly of Pliocene to Pleistocene age. This indicates that the accretionary prism is covered by thick (in part probably more than 1 km) sequences of late Tertiary and Quaternary sediments.

In consideration of the wide range of sedimentary structures and dominant grain size (matrix- to grain-supported, poorly to moderately rounded (brecciated) clasts, laminations, graded bedding, slump folds, load and dewatering structures), we interpret the majority of the slope samples as originally representing hemipelagic sediments reworked by mass and fluidal flows such as slumps and slides, debris and mud flows, and low-density turbidites. Dewatering structures at the contact of mud flows with underlying older strata indicate rapid deposition. The age model of ODP Site 1232, located in the Chile basin at 40°S, shows that the recurrence time of turbidites is in the order of centuries, possibly caused by earthquakes and instabilities at the continental slope associated with climate-induced variabilities in sediment supply from the continent (Mix et al., 2003).

The degree of sediment reworking on the slope appears to be high, an assumption which is supported by

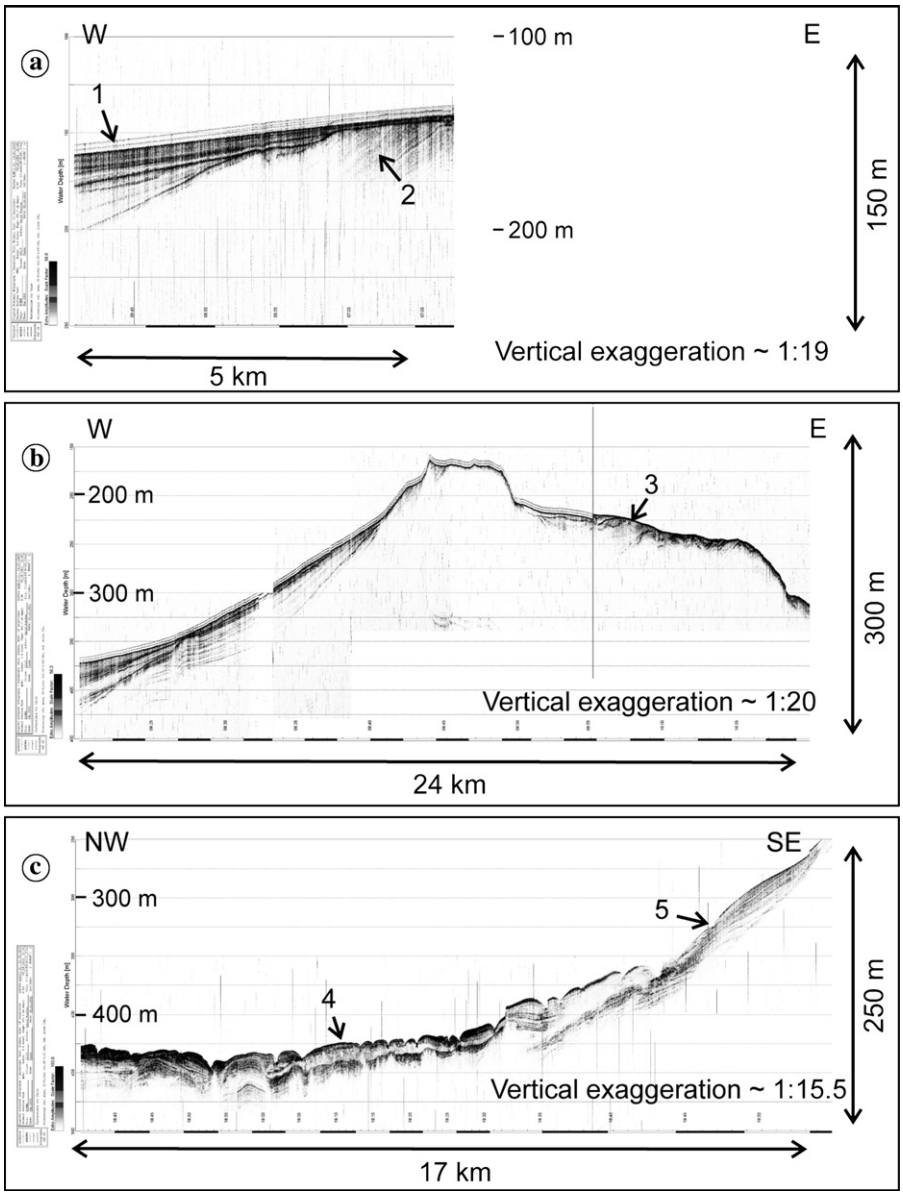

Fig. 9. Examples of typical PARASOUND sediment-echosounder profiles of the outer shelf and uppermost continental slope off southern central Chile. Locations of profiles are shown in Fig. 1. a) Disconformable onlap of a thin, young sedimentary cover (1) on erosionally truncated strata (foresets) on the outer shelf (2). The older strata form the seafloor of the shelf landward of the profile. b) Uppermost slope and outer shelf at 36°S. The shelf edge and outer shelf are characterized by low signal penetration, and deformed strata which are indicative for the absence of unconsolidated sediments (3). This is the predominant acoustic facies on the outer shelf. The vertical line indicates an adjustment of the acoustic signal. c) Deformed strata (slump mass) on the upper slope (4). The slump mass seems to have detached from the upper shelf with the slump scar (5) still being exposed.

the occurrence of numerous small-scale erosional unconformities and the abundant occurrence of semi-consolidated rip-up mud clasts near the bases of small-scale debris flows and turbidites (Fig. 3a). The rip-up clasts, despite being only moderately consolidated, are commonly only poorly rounded, thus suggesting short transport distances (probably in the order of a few m).

In addition, incoherent reflection patterns in PARASOUND records (Wiedicke-Hombach and Shipboard Scientific Party, 2002) from steep parts of the submarine slope point to disturbed bedding and to large-scale mass-wasting processes affecting the morphology and dynamics of the submarine slope (Fig. 9). The regional high seismicity may readily trigger slumping and

debris flows on the structurally unstable slope which pass downslope into mud flows and turbidity currents.

The nature of the well-rounded gravels dredged from the upper slope (104 KD) is enigmatic. Their shape suggests reworking either by fluvial or coastal transport, but the most likely way to transport them across the shelf to their present location at a water depth of 580–390 m is by glaciers or icebergs. Gravels of similar appearance are found on the shelf.

5.1.5. Sedimentation in slope basins

PARASOUND and seismic records assisted in distinguishing slope sedimentary environments from slope basins. Slope basins are in contrast to the steep slope parts characterized by coherent parallel reflection patterns, indicating the accumulation of thick undisturbed sequences of hemipelagic sediments with occasionally interbedded distal turbidites, which are best preserved in protected slope basins where erosion and reworking of sediments by gravity mass movements are limited. This assumption is supported by Sites 1233, 1234, and 1235 of ODP Leg 202 (Mix et al., 2003), which were drilled in flat-topped basins on the upper slope (Fig. 1), and represent almost turbidite-free hemipelagic sequences. The up to 240 mcd (measured composite depth) thick sediment sequences are all younger than 260 ka. The resulting sedimentation rates are extremely high. Hemipelagic sedimentation in slope basins is shown to be nearly continuous, with average sedimentation rates of 70 to 82 cm/ka within the last 260 ka, and maximum values of up to 160 cm/ka (Mix et al., 2003).

5.1.6. Sedimentation in submarine canyons

Dredge samples from the floor and walls of the Bío-Bío, Toltén, Calle-Calle, and Bueno canyons are characterized by a higher degree of lithification and coarser grain size compared to slope dredge samples, up to cobble-dominated gravels. Secondly, samples from the canyon walls show a spectrum of sedimentary structures characteristic of gravity flow and mass-wasting processes from slumping, mud-, and debris flows, through grain- and liquefied flows to turbidity currents of high and low density. This is in accordance with sedimentological analysis of cores obtained from the bottom of the Bío-Bío canyon segment that cuts into the shelf, which reveal the presence of turbidites, generated by slumping and debris flows (Pineda, 1999).

We interpret this as an indicator of high-energy downslope transport processes focussed to the canyons. In the Bío-Bío canyon, theses processes are induced by the bedload of the Bío-Bío river (Pineda, 1999). It has been shown, that turbidity currents can cross the Chile Trench and produce turbiditic beds on the summit of seamounts which are up to 300 m high and 25 km away from the continental foot (Völker et al., 2006).

5.1.7. Distribution pattern of clay minerals

(Hemi-)pelagic sediments from the continental slope show a distribution pattern of clay minerals with respect to the distance from the coast (Fig. 8) and therefore also with sedimentary environment. The chlorite proportion of clay minerals increases from the lower slope to the upper slope, corresponding with a decrease in the proportion of smectite. The illite proportion reaches its maximum on the middle slope. This fractionation may be due to predominant grain size and due to different affinities to flocculation effects. Clay minerals suspended in fresh water tend to form aggregates during mixing with salt water upon entering the sea. This is due to van der Waals forces or electrostatic attraction, resulting in large aggregates and faster settling. Einsele (2000) described that kaolinite tends to flocculate near the river mouths and begins to sink whereas illite and montmorillonite (smectite) are transported further offshore. A similar distribution pattern was described by several authors (e.g., Carson and Arcaro, 1983; Gibbs, 1985), and also by Lamy et al. (1998) for the 36° transect of the southern central Chilean continental margin.

5.2. Accretion and subduction

As mentioned in Section 4.1, neither rocks of oceanic affinity nor sediments predating Miocene were dredged (Table 1), although walls of deeply incised canyons were sampled specifically to that purpose. This suggests that lithologies associated with oceanic crust are not incorporated into the accretionary wedge, but subducted completely. This conclusion is consistent with seismic evidence from Bangs and Cande (1997) who demonstrated that the basal detachment in the study region lies up to several hundred meters above the oceanic crust, and is also consistent with the geochemical results of Hickey-Vargas et al. (2002) and Sigmarsson et al. (1990) which showed that the Andean arc magma has been contaminated by subducted sediments for the last 10 Ma.

If our interpretation of the genesis of one sample from 114 KD and it's age dating is correct (Table 1), sediment that was formed in a sediment fan at the base of the continental slope about 2.5 Ma ago, is now exposed on the lower slope, some 17 km landward of the deformation front and in a water depth of ~2700 m. This would imply that the sediment was incorporated into the accretionary wedge and slowly lifted as new sediment stacks were added to the frontal prism subsequently. It

would also imply that at least the leading 17 km of the accretionary wedge were built within the last ~2.5 Ma. This corresponds to an accreted volume of ~16 km^3/km/Ma which is considerably lower than the value of 71 to 77 km^3/km/Ma calculated by Bangs and Cande (1997).

When considering the contrast between these high accretion rates and the relatively small accretionary wedge of south-central Chile, long periods of subduction erosion could serve as an explanation for maintaining a small accretionary prism in light of high accretion rates. Large parts of the accretionary wedge may have been eroded and subducted during interglacial stages when the trench was not sufficiently supplied with sediments (Bangs and Cande, 1997). The study of Melnick and Echtler (2006) shows that the onset of glacial age trench fill associated with the global cooling (~6 Ma ago) shifted the margin off south-central Chile from erosive to accretionary during the middle Pliocene.

5.3. Diagenesis and burial depths

As described in Section 4.1.4, many samples were affected by early diagenetic lithification and deformed shortly after deposition. XRD analysis indicates high concentration of calcite in all samples and thin sections show that calcite is the principal cement mineral. In some cases, low pyrite contents, determined by XRD analysis, point to biochemical sulfate reduction as the cementing process. This finding is in agreement with observations from ODP Site 1235 where authigenic pyrite and carbonate are present, especially in deeper intervals (Mix et al., 2003). In a common reaction, chemosynthesizing organisms reduce sulfate and organic matter to hydrogen sulfide and hydrogen carbonate ($SO_4^{2-} + 2\ CH_2O \rightarrow H_2S + 2\ HCO_3^-$), providing the base for early diagenetic calcite and pyrite formation (Berner, 1980; Hesse, 1986). In contrast, we did not find any evidence of very-low-grade metamorphic reactions, indicated by index minerals such as stilpnomelane, pyrophyllite, or laumontite.

Sample 62 KD shows the highest degree of lithification (Fig. 3b) because it is completely dolomitized, lacking any calcite. Borehole data from ODP Leg 202 (Mix et al., 2003) showed increasing dolomite precipitation from 40 m to 230 mbsf, downhole of which dolomitization is complete. We therefore assume that this sample was buried to a minimum depth of 40 m but more likely to ~230 mbsf before being exposed at the surface. Because no other lithologically similar dredge sample contains dolomite to a significant degree, current surface samples available for sampling and dredging probably never reached the depth of dolomite precipitation. The cycle of sedimentation, subsidence, diagenesis, uplift, erosion, and resedimentation on the accretionary prism in south-central Chile therefore takes place within the upper ~230 mbsf of the continental slope.

6. Summary and conclusions

From our petrological and sedimentological studies supported by the interpretation of PARASOUND-echosounder profiles, we conclude that:

(1) The shelf is starved of young, unconsolidated sediments. The character of sediments on the outer shelf indicates a high degree of reworking, winnowing, and transport to the uppermost slope. The combination of submarine canyons deeply cutting into the shelf and strong bottom currents assures that only a very small fraction of the abundant fluvial sedimentary load escapes transport to the slope and finally to the trench.
(2) None of the dredge samples from the walls of deeply incised submarine canyons was dated older than Pliocene. These sites are located some hundred meters (up to 1000 m) below the general slope surface on steep canyon walls. Hence, the continental slope, in contrast to the shelf edge, is likely covered by thick sequences of late Tertiary and Quaternary sediments.
(3) A large range of mass-wasting processes act on the submarine slope with a dominance of slumps or debris flows, evolving to low-density turbidity currents and mud flows. Slope bathymetry and the abundance of erosion and transport processes acting on semi-consolidated sediments give the impression that slope stability is generally low. It seems probable that submarine slumps are periodically triggered by earthquakes with a recurrence time in the order of centuries. These mass-wasting processes are responsible for the rare exposure of sediments which have been buried up to several hundred meters. In contrast, slope basins are largely filled with undisturbed hemipelagic sediments.
(4) Several large submarine canyon systems form preferred pathways for efficient sediment transport to the trench, particularly for coarse-grained material in channelized high-density turbidity currents and debris flows.
(5) Sediments on the slope are lithified early, possibly dominated by biochemical sulfate reduction processes.
(6) The latitudinal petrographic change in sandstone petrographic composition shows a southward

increase of metamorphic rock fragments from the Late Paleozoic accretionary complex in Coastal Cordillera and a corresponding southward decrease of volcanic rock fragments. This reflects a southward increase in the denudation of the hinterland, mainly due to the increase in precipitation rates and a higher degree of Pleistocene glaciation.

(7) Systematic compositional abundance variations of clay minerals with distance to the coast is related to different flocculation behavior, resulting in different settling times and transport widths.

(8) The cycle of sedimentation, subsidence, diagenesis, uplift, erosion, and resedimentation on the accretionary prism in south-central Chile seems to take place within the upper ~230 mbsf of the continental slope.

Acknowledgments

Many thanks go to the Shipboard Scientific Party and crew of the *R/V SONNE* for their support during the cruise SO161-5 part of the BMBF-funded Project SPOC (Subduction Processes Off Chile). We also thank the Federal Institute for Geosciences and Natural Resources (BGR) in Hannover for staffing the cruise, and chief scientist Michael Wiedicke-Hombach for supplying us with the dredge samples. The editor David J.W. Piper and two anonymous reviewers are gratefully acknowledged for helpful and constructive reviews of the manuscript.

References

Angermann, D., Klotz, J., Reigber, C., 1999. Space-geodetic estimation of the Nazca–South American Euler vector. Earth Planet. Sci. Lett. 171, 329–334.

Arkaí, P., 1991. Chlorite crystallinity: an empirical approach and correlation with illite crystallinity, coal rank and mineral facies as exemplified by Palaeozoic and Mesozoic rocks of northeast Hungary. J. Metamorph. Geol. 9, 723–734.

Bangs, N., Cande, S.C., 1997. Episodic development of a convergent margin inferred from structures and processes along the southern Chile margin. Tectonics 16 (3), 489–503.

Barron, J.A., 1985. Miocene to Holocene planktonic diatoms. In: Bolli, H.M., Saunders, J.B., Perch-Nielsen, K. (Eds.), Plankton Stratigraphy. Cambridge University Press, Cambridge, pp. 763–809.

Berner, R.A., 1980. Early Diagenesis. A Theoretical Approach. Princeton University Press, N. J. 256 pp.

Bohm, M., Lüth, S., Echtler, H., Asch, G., Bataille, K., Bruhn, C., Rietbrock, A., Wigger, P., 2002. The Southern Andes between 36° and 40°S latitude: seismicity and average seismic velocities. Tectonophysics 356, 275–289.

Braukmann, F.J., 1984. Hochdiagenese im Muschelkalk der Massive von Bramsche und Vlotho. Bochum. Geol. Geotechn. Arb. 14 (195 pp.).

Carson, B., Arcaro, N.P., 1983. Control of clay mineral stratigraphy by selective transport in Late Pleistocene–Holocene sediments of northern Cascadia basin–Juan de Fuca abyssal plain: implication for studies of clay mineral provenance. J. Sediment. Petrol. 53, 395–406.

Dahlen, F.A., 1990. Critical taper model of fold-and-thrust belts and accretionary wedges. Annu. Rev. Earth Planet. Sci. 18, 55–99.

Deruelle, B., 1982. Petrology of the Plio–Quartenary volcanism of the south-central and meridional Andes. J. Volcanol. Geotherm. Res. 17, 97–124.

Dewey, J.F., Bird, J.M., 1970. Mountain belts and the new global tectonics. J. Geophys. Res. 75, 2625–2647.

Díaz-Naveas, J.L., 1999. Sediment subduction and accretion at the Chilean convergent margin between 35° und 40°S. Ph.D. Thesis, Ch.-A.-Universität, Kiel, 130 pp.

Dickinson, W.R., 1985. Interpreting provenance relations from detrital modes of sandstones. In: Zuffa, G.G. (Ed.), Provenance of Arenites. D. Reidel Publishing Company, Dordrecht, Boston, Lancaster, pp. 333–361.

Eberl, D.D., Srodon, J., Lee, M., Nadeau, P.H., Northrop, H.R., 1987. Sericite from the Silverton caldera, Colorado: correlation among structure, composition, origin, and particle thickness. Am. Mineral. 72, 914–934.

Einsele, G., 2000. Sedimentary basins: evolution, facies, and sediment budget. Springer-Verlag, Berlin, Heidelberg. 791 pp.

Ferguson, I.J., Westbrook, G.K., Langseth, M.G., Thomas, G.P., 1993. Heat flow and thermal models of the Barbados Ridge accretionary complex. J. Geophys. Res. 98, 4121–4142.

Gazzi, P., 1966. Le arenie del flysch sopracretaceo dell' Apenino modense: correlazione con il flysch di Monghidoro. Mineral. Petrogr. Acta 16, 69–97.

Gibbs, R.J., 1985. Settling velocity, diameter, and density for flocs of illite, kaolinite und montmorillonite. J. Sediment. Petrol. 55, 65–68.

Grevemeyer, I., Díaz-Naveas, J.L., Ranero, C.R., Villinger, H.W., Ocean Drilling Program Leg 202 Scientific Party, 2003. Heat flow over the descending Nazca Plate in central Chile, 32° to 41°S: observations from ODP Leg 202 and the occurrence of natural gas hydrates. Earth Planet. Sci. Lett. 213, 285–298.

Hesse, R., 1986. Diagenesis 11. Early diagenetic pore water/sediment interaction: modern offshore basins. Geosci. Can. 13, 165–196.

Hickey-Vargas, R., Sun, M., López-Escobar, L., Moreno-Roa, H., Reagan, M.K., Morris, J.D., Ryan, J.G., 2002. Multiple subduction components in the mantle wedge: evidence from eruptive centers in the Central Southern volcanic zone, Chile. Geology 30 (3), 199–202.

Hine, N., Weaver, P.P.E., 1998. Quaternary. In: Bown, P.R. (Ed.), Calcareous Nannofossil Biostratigraphy. Chapman and Hall, pp. 266–283.

Homrighausen, R., 1979. Petrographische Untersuchungen an sandigen Gesteinen der Hörre-Zone (Rheinisches Schiefergebirge, Oberdevon-Unterkarbon). Geol. Abh. Hess. 79 (84 pp.).

Huyer, A., Kosro, P.M., Fleischbein, J., Ramp, S.R., Stanton, T., Washburn, L., Chavez, F.P., Cowles, T.J., Pierce, S.D., Smith, R.L., 1991. Currents and water masses of the coastal transition zone off northern California, June to August 1988. J. Geophys. Res. 96, 14809–14831.

Hyndman, R.D., Wang, K., Yuan, G.D., 1993. Spence, tectonic sediment thickening, fluid expulsion, and the thermal regime of subduction zone accretionary prisms: the Cascadia margin off Vancouver Island. J. Geophys. Res. 98, 21865–21876.

Ingersoll, R.V., Bullard, T., Ford, R., Grimm, J., Pickle, J., Sares, S., 1984. The effect of grain size on the detrital modes: a test of the

Gazzi–Dickinson point-counting method. J. Sediment. Petrol. 54, 103–116.
Kisch, H.J., 1991. Illite crystallinity: recommendations on sample preparation, X-ray diffraction settings, and interlaboratory samples. J. Metamorph. Geol. 9, 665–670.
Lamy, F., Hebbeln, D., Wefer, G., 1998. Terrigeneous sediment supply along the Chilean continental slope: modern latitudinal trends of texture and composition. Geol. Rundsch. 87, 477–494.
Lamy, F., Hebbeln, D., Röhl, U., Wefer, G., 2001. Holocene rainfall variability in southern Chile: a marine record of latitudinal shifts of the southern Westerlies. Earth Planet. Sci. Lett. 185, 369–382.
Laursen, J., Normark, W.R., 2002. Late Quaternary evolution of the San Antonio Submarine Canyon in the central Chile forearc (~33°S). Mar. Geol. 188, 365–390.
Lezzerini, M., Sartori, F., Tamponi, M., 1995. Effect of amount of material used on sedimentation slides in the control of illite "crystallinity" measurements. Eur. J. Mineral. 7, 819–823.
Lindquist, K., Engle, K., Stahlke, D., Price, E., 2004. Global topography and bathymetry grid improves research efforts. EOS 85 (19). doi:10.1029/2004EO190003.
Lohrmann, J., Kukowski, N., Krawczyk, C.M., Oncken, O., Sick, C., Sobiesiak, M., Rietbrock, A., 2006. Subduction channel evolution in brittle fore-arc wedges — a combined study with scaled sandbox experiments, seismological and reflection seismic data and geological field evidence. In: Oncken, O., Chong, G., Franz, G., Giese, P., Götze, H.-J., Ramos, V.A., Strecker, M.R., Wigger, P. (Eds.), The Andes — Active Subduction Orogeny. Frontiers in Earth Sciences. Springer, Berlin Heidelberg, pp. 237–262.
Melnick, D., Echtler, H.P., 2006. Inversion of forearc basins in south-central Chile caused by rapid glacial age trench fill. Geology 34 (9), 709–712.
Mercer, J.H., 1976. Glacial history of the southernmost South America. Quat. Res. 6, 125–166.
Mix, A.C., Tiedemann, R., Blum, P., et al., 2003. Proc. ODP, Init. Repts., 202. Available from World Wide Web: http://www-odp.tamu.edu/publications/202_IR/202ir.htm.
Muñoz, P., Lange, C.B., Gutiérrez, D., Hebbeln, D., Salamanca, M.A., Dezileau, L., Reiss, J.L., Benninger, L.K., 2004. Recent sedimentation and mass accumulation rates based on 210Pb along the Peru–Chile continental margin. Deep-Sea Res. II 51, 2523–2541.
Perch-Nielsen, K., 1985. Cenozoic calcareous nannofossils. In: Bolli, H.M., Saunders, J.B., Perch-Nielsen, K. (Eds.), Plankton Stratigraphy. Cambridge University Press, Cambridge, pp. 427–554.
Pineda, V., 1999. El cañón submarino del Bío-Bío: aspectos dinámicos y ambientales. Ph.D. Thesis, Universidad de Concepción, Chile, 105 pp.
Pineda, V., Fanucci, F., 1994. El cañón submarino del Bío-Bío y su importancia en la dinámica y equilibrio del litoral del golfo de Arauco, Concepción, Chile. 7° Congreso Geológico Chileno, vol. 1, pp. 371–374.
Pizarro, O., Shaffer, G., Dewitte, B., Ramos, M., 2002. Dynamics of seasonal and interannual variability of the Peru–Chile Undercurrent. Geophys. Res. Lett. 29 (12). doi:10.1029/2002GL014790.
Plafker, G., 1972. Alaskan earthquake of 1964 and Chilean earthquake of 1960; implications for arc tectonics. J. Geophys. Res. 77, 901–925.
Rabassa, J., Clapperton, C.M., 1990. Quaternary glaciations of the southern Andes. Quat. Sci. Rev. 9, 153–174.
Ranero, C.R., von Huene, R., Weinrebe, W., Reichert, C., 2006. Tectonic processes along the Chile convergent margin. In: Oncken, O., Chong, G., Franz, G., Giese, P., Götze, H.-J., Ramos, V.A., Strecker, M.R., Wigger, P. (Eds.), The Andes — Active Subduction Orogeny. Frontiers in Earth Sciences. Springer, Berlin Heidelberg, pp. 91–123.
Rauch, K., 2005. Cyclicity of Peru–Chile trench sediments between 36° and 38°S: a footprint of paleoclimatic variations? Geophys. Res. Lett. 32, L08302. doi:10.1029/2004GL022196.
Scholl, D.W., Christensen, M.N., von Huene, R., Marlow, M.S., 1970. Peru–Chile trench. Sediments and sea-floor spreading. Geol. Soc. Amer. Bull. 81, 1339–1360.
SERNAGEOMIN, 2003. Mapa Geológico de Chile: versión digital. Servicio Nacional de Geología y Minería, Publicación Geológica Digital, No. 4 (CD-ROM, versión 1.0, 2003). Santiago.
Shaffer, G., Salinas, S., Pizarro, O., Vega, A., Hormazábal, S., 1995. Currents in the deep ocean off Chile. Deep-Sea Res. II 42, 425–436.
Shaffer, G., Pizarro, O., Djurfeldt, L., Salinas, S., Rutllant, J., 1997. Circulation and low frequency variability near the Chile coast: remotely-forced fluctuations during the 1991–1992 El Niño. J. Phys. Oceanogr. 27, 217–235.
Shaffer, G., Hormazábal, S., Pizarro, O., Salinas, S., 1999. Seasonal and interannual variability of currents and temperature off central Chile. J. Geophys. Res. 104, 29951–29961.
Sick, C., Yoon, M.-K., Rauch, K., Buske, S., Lüth, S., Araneda, M., Bataille, K., Chong, G., Giese, P., Krawczyk, C., Mechie, J., Meyer, H., Oncken, O., Reichert, C., Schmitz, M., Shapiro, S., Stiller, M., Wigger, P., 2006. Seismic images of accretive and erosive subduction zones from the Chilean margin. In: Oncken, O., Chong, G., Franz, G., Giese, P., Götze, H.-J., Ramos, V.A., Strecker, M.R., Wigger, P. (Eds.), The Andes — Active Subduction Orogeny. Frontiers in Earth Sciences. Springer, Berlin Heidelberg, pp. 147–171.
Sigmarsson, O., Condomines, M., Morris, J.D., Harmon, R.S., 1990. Uranium and ^{10}Be enrichments by fluids in Andean arc magmas. Nature 346, 163–165.
Smith, W.H.F., Sandwell, D.T., 1997. Global seafloor topography from satellite altimetry and ship depth soundings. Science 277, 1957–1962.
Strub, P.T., Mesias, J.M., Montecino, V., Rutllant, J., Salinas, S., 1998. Coastal ocean circulation off Western South America. In: Robinson, A.R., Brink, K.H. (Eds.), The Global Coastal Ocean. Wiley, New York, pp. 273–314.
Thiele, R., Moreno, H., Elgueta, S., 1998. Evolución geológico-geomorfológica cuaternaria del tramo superior del valle del río Laja. Rev. geol. Chile 25 (2), 229–253.
Thornburg, T.M., Kulm, L.D., 1987a. Sedimentation in the Chile trench: depositional morphologies, lithofacies, and stratigraphy. Geol. Soc. Amer. Bull. 98, 33–52.
Thornburg, T.M., Kulm, L.D., 1987b. Sedimentation in the Chile trench: petrofacies and provenance. J. Sediment. Petrol. 57, 55–74.
Thornburg, T.M., Kulm, L.D., Hussong, D.M., 1990. Submarine-fan development in the southern Chile trench: a dynamic interplay of tectonics and sedimentation. Geol. Soc. Amer. Bull. 102, 1658–1680.
Vargas, I., 2005. Análisis morfo-estructural, sedimentológico y geoquímica del margen continental chileno entre los 36°–47°S. Thesis, Departamento Ciencias de la Tierra, Universidad de Concepción, Chile, 121 pp.
Vargas, I., Pineda, V., Fanucci, F., 2005. Morpho-structural features of the Chilean continental margin from 36°–37°S. VIII International Conference on Gas Marine Sediments (September 5–10), Vigo, España.
Völker, D., Wiedicke, M., Ladage, S., Gaedicke, C., Reichert, C., Rauch, K., Kramer, W., Heubeck, C., 2006. Latitudinal variation in sedimentary processes in the Peru–Chile trench off Central Chile. In: Oncken, O., Chong, G., Franz, G., Giese, P., Götze, H.-J., Ramos, V.A., Strecker, M.R., Wigger, P. (Eds.), The Andes —

Active Subduction Orogeny. Frontiers in Earth Sciences. Springer, Berlin Heidelberg, pp. 193–216.

von Huene, R., Corvalan, J., Flueh, E.R., Hinz, K., Korstgard, J., Ranero, C.R., Weinrebe, W., Klaeschen, D., Naveas, J.L.D., Harms, G., Spiegler, D., Biebow, N., Locker, S., Kruger, D., Morales, E., Vergara, H., Yanez, G., Valenzuela, E., Wall, R., Trinhammer, P., Laursen, J., Scholl, D., Kay, S., Dominguez, S., Segl, M., Beese, D., Lamy, F., Bialas, J., Biegling, A., Gerdom, M., Hojka, A.M., Hoppenworth, R., Husem, S., Krastel, S., Kulowski, N., Morawe, M.P., Munoz, A.E.D., Lefmann, A.K., Vidal, N.M., Zelt, C., Hinz, K., Block, M., Damm, V., Fritsch, J., Neben, S., Reichert, C., Schreckenberger, B., 1997. Tectonic control of the subducting Juan Fernandez Ridge on the Andean margin near Valparaiso, Chile. Tectonics 16 (3), 474–488.

von Huene, R., Lallemand, S., 1990. Tectonic erosion along the Japan and Peru convergent margins. Geol. Soc. Amer. Bull. 102, 704–720.

von Huene, R., Scholl, D.W., 1991. Observations at convergent margins concerning sediment subduction, subduction erosion, and the growth of continental crust. Rev. Geophys. 29, 279–316.

von Huene, R., Kulm, L.D., Miller, J., 1985. Structure of the frontal part of the Andean convergent margin. J. Geophys. Res. 90, 5429–5442.

von Huene, R., Weinrebe, W., Heeren, F., 1999. Subduction erosion along the North Chile margin. Geodynamics 27, 345–358.

Warr, L.N., Rice, H.N., 1994. Interlaboratory standardization and calibration of clay mineral crystallinity and crystallite size data. J. Metamorph. Geol. 12, 141–152.

Wiedicke-Hombach, M., Shipboard Scientific Party, 2002. Cruise Report SO161-5 SPOC (Subduction Processes Off Chile), Geology–Geochemistry-Heatflow. Archive, vol. 11241/02. BGR, Hannover.

Young, J.R., 1998. Neogene. In: Bown, P.R. (Ed.), Calcareous Nannofossil Biostratigraphy. Chapman and Hall, pp. 225–265.

Zapata, R.A., 2001. Estudio batimétrico del margen Chileno. Thesis, Faculdad de Ciencias Fisicas y Matematicas, Departamento de Geofisica, Universidad de Chile, Santiago de Chile, 113 pp.